Phonon-Polariton Mediated Thermal Radiation and Heat Transfer among Molecules and Macroscopic Bodies: Nonlocal Electromagnetic Response at Mesoscopic Scales

Prashanth S. Venkataram,[1] Jan Hermann,[2] Alexandre Tkatchenko,[2] and Alejandro W. Rodriguez[1]

[1]*Department of Electrical Engineering, Princeton University, Princeton, New Jersey 08544, USA*
[2]*Physics and Materials Science Research Unit, University of Luxembourg, L-1511 Luxembourg*

Thermal radiative phenomena can be strongly influenced by the coupling of phonons and long-range electromagnetic fields at infrared frequencies. Typically employed macroscopic descriptions of thermal fluctuations often ignore atomistic effects that become relevant at nanometric scales, whereas purely microscopic treatments ignore long-range, geometry-dependent electromagnetic effects. We describe a mesoscopic framework for modeling thermal fluctuation phenomena among molecules near macroscopic bodies, conjoining atomistic treatments of electronic and vibrational fluctuations obtained from density functional theory in the former with continuum descriptions of electromagnetic scattering in the latter. The interplay of these effects becomes particularly important at mesoscopic scales, where phonon polaritons can be strongly influenced by the objects' finite sizes, shapes, and nonlocal or many-body response to electromagnetic fluctuations. We show that, even in small but especially in elongated low-dimensional molecules, such effects can modify thermal emission and heat transfer by orders of magnitude and produce qualitatively different behavior compared to predictions based on local, dipolar, or pairwise approximations.

Radiative heat transfer is important when characterizing molecular structures, including graphene, fullerenes, carbon nanotubes, and other low-dimensional materials, and has applications to thermophotovoltaic power generation [1–4], lasers [5,6], and single-molecule junctions [7,8]. Recent theoretical [9–11] and experimental [12–15] works in this area have explored transport at nanometric scales, where the interplay of electromagnetic (EM) and phonon mediated transport can no longer be captured solely by macroscopic electrodynamics [12–14]. We present a framework for modeling thermal fluctuation phenomena among molecules near continuum bodies at mesoscopic scales and apply it to compute heat transfer between molecules in contact with separate thermal reservoirs. Our approach captures the emergence of phonon polaritons [16,17], which typically arise at infrared frequencies and hence probe the bulk of the Planck distribution near room temperature, and their impact on charge delocalization (nonlocality) and radiation. By extending microscopic *ab initio* models of electronic response in molecular bodies based on density functional theory (DFT) to include molecular vibrations mediated by short-range interactions (phonons), and combining these with classical EM scattering techniques applicable to *arbitrary* macroscopic objects [18,19], we account for their coupling to collective electronic excitations (plasmon polaritons), including retardation, multiple scattering, and geometry-dependent many-body effects to all orders. Our framework, detailed below, assumes the Born-Oppenheimer approximation for the nuclear motion and a harmonic approximation to the chemical bonds effecting molecular

phonons and ignores thermally driven changes in molecular conformations, all of which are only expected to be violated at large temperatures. For illustration, we investigate thermal emission and heat transfer among fullerene and carbyne molecules at different temperatures, either in vacuum or above a metallic surface. We find differences of over an order of magnitude in the emitted and transferred powers relative to common dipolar approximations that neglect finite size and many-body EM effects, with the greatest differences obtained for elongated carbyne wires. We show that the proximity of the molecules to the metallic surface and resulting induction of image charges can qualitatively change their mutual heat transfer. More interestingly, we find that molecular phonon polaritons can delocalize the spatial extent of their polarization response, from a few angstroms up to tens of nanometers, depending on the shape of the molecules and their proximity to the surface. Such nonlocality qualitatively changes the heat transfer (eventually saturating) at nanometric scales.

Recent theoretical models accounting for atomic-scale and vibrational effects on radiative emission and heat transfer suffer from a number of limitations [6,20–27]. Commonly, atomistic mechanical Green's functions [10,12,16,17,28,29] are used to model phonon mediated transport across material boundaries. While the harmonic spring constants that lead to collective mechanical oscillations have recently been derived through DFT methods, they have thus far only been applied to bulk media, whereas heat transport across vacuum gaps or in structured media has been largely ignored or approximated through *ad hoc*

pairwise models known to fail in complex geometries [30–34]. Other atomistic methods include molecular dynamics [9,35–37], which capture the anharmonicity of covalent bonds but suffer from similar pitfalls of heuristically approximating noncovalent interactions. Macroscopic approaches based on fluctuational electrodynamics arise from discrete dipolar and multipolar methods [11,38–41] and other continuum EM treatments based on discretization of bulk susceptibilities and fields [1–3,18,19,42–49], which discretize bulk susceptibilities using point dipoles or other basis functions. While such methods capture the impact of long-range EM effects, they typically treat material responses at atomic scales via semiempirical models rather than *ab initio* calculations and can therefore miss important effects arising from the spatial dispersion or nonlocality of electronic wave functions and its interplay with geometry. Even for a material like graphene with highly delocalized electronic and mechanical response [2,50–52], nonlocality is typically treated phenomenologically through macroscopic approximations of quantum behavior. Motivated by recent predictions [31–34,53] of many-body van der Waals (vdW) interactions in low-dimensional systems and experiments investigating heat transfer at the nanoscale [12–15,54], both of which probe regimes where continuum electrodynamics may no longer be valid, we propose a framework that can capture such thermal radiative processes at mesoscopic scales.

Background.—We consider a collection of N_{mol} molecules labeled k and described by electric susceptibilities $\mathbb{V}_k$ in the presence of a collection of macroscopic bodies described collectively by a macroscopic susceptibility $\mathbb{V}_{\mathrm{env}}$, relating induced polarization and electric fields; the former are maintained at temperatures T_k, and the latter is maintained at a different temperature T_{env} (henceforth assumed to be zero for conceptual convenience). The radiative energy transfer from molecule m to n (which may or may not be the same), can be shown to be [55]

$$\Phi_n^{(m)} = -\frac{1}{2\pi}\mathrm{Tr}[\mathrm{Im}(\mathbb{V}_m^{-1\star})\mathbb{P}_m\mathbb{T}^\star\mathrm{asym}(\mathbb{P}_n\mathbb{G}_{\mathrm{env}})\mathbb{T}\mathbb{P}_m], \quad (1)$$

where $\mathbb{T}^{-1} = \sum_k \mathbb{V}_k^{-1} - \mathbb{G}_{\mathrm{env}}$ is known as a scattering transition operator, which describes EM scattering (to all orders) by the collection of molecules in the presence of all bodies [43,57]. $\mathbb{G}_{\mathrm{env}} = (\mathbb{G}_0^{-1} - \mathbb{V}_{\mathrm{env}})^{-1}$ is the classical EM Green's function [43,53,57], and $\mathbb{P}_k$ projects onto the space spanned by the degrees of freedom of molecule k. Here, $\star$ implies complex conjugation, $\dagger$ implies conjugate transposition (adjoint), $\mathrm{Im}(\mathbb{A}) = (\mathbb{A} - \mathbb{A}^\star)/(2i)$, and $\mathrm{asym}(\mathbb{A}) = (\mathbb{A} - \mathbb{A}^\dagger)/(2i)$. Given (1), the far-field thermal emission from molecule m,

$$W^{(m)} = \sum_{n=1}^{N} s_{nm}\Phi_n^{(m)}\Theta(\omega, T_n), \quad (2)$$

and the net heat transfer from molecule m to molecule n,

$$W_{m\to n} = \Phi_n^{(m)}[\Theta(\omega, T_m) - \Theta(\omega, T_n)], \quad (3)$$

where $\Theta(\omega, T)$ is the Planck function, while the sign function $s_{nm} = 1 - 2\delta_{nm}$ accounts for the direction of energy flow for the emission of a body. In either case, the net power is the integral over all frequencies, $P = \int_0^\infty W(\omega)d\omega$.

The above formulas require accurate and fast computations of $\mathbb{G}_{\mathrm{env}}$ and $\mathbb{V}_k$. The former can be computed using any number of state-of-the-art classical EM techniques for arbitrary macroscopic geometries, including spectral, boundary element, or finite-difference methods [18,19,46–49]. The molecular susceptibilities $\mathbb{V}_k$ generally require quantum descriptions, but recent work in the related field of vdW interactions [30,32,33,58] has shown that accurate models of the valence electronic response of insulating or weakly metallic molecules, including carbon allotropes, can be obtained by expressing $\mathbb{V}_k = \sum_{p,q}\alpha_{pi,qj}|f_p\mathbf{e}_i\rangle\langle f_q\mathbf{e}_j|$ in a localized basis $|f_p\rangle$ (along Cartesian direction $\mathbf{e}_i$) associated with each atom p by modeling its valence electrons as a quantum oscillator in its ground state. We extend that framework in the following way: each atom p in a given molecule comprises an effective valence electron that couples to long-range EM fields and has charge q_p, mass m_{ep}, and damping coefficient $b_{ep} = m_{ep}\gamma_{ep}$, as well as a nucleus of mass m_{Ip} which is coupled only to its associated valence electron with spring constant k_{ep} and to neighboring nuclei [5,16,17,25] with spring constants $\mathbb{K}_{pq}$. While m_{Ip} are obtained from elemental data and γ_{ep} come from empirical data [59], m_{ep}, q_p, k_{ep}, and $\mathbb{K}_{pq}$, along with the molecular geometries, are all obtained from DFT [32,34] (see Supplemental Material [55] for more details), thereby accounting for short-range electrostatic, hybridization, and quantum exchange effects. The nuclear harmonic couplings, in particular, arise from lowest-order expansions of DFT force constants, producing anisotropy (tensorial couplings) due to the directionality of covalent bonds. This leads to the simple frequency-domain equations of motion

$$\begin{bmatrix} K_e - i\omega B_e - \omega^2 M_e & -K_e \\ -K_e & K_e + K_I - \omega^2 M_I \end{bmatrix}\begin{bmatrix} x_e \\ x_I \end{bmatrix} = \begin{bmatrix} Q_e e_e \\ 0 \end{bmatrix}, \quad (4)$$

where $(Q_e, M_e, M_I, K_e, K_I, B_e)$ are $3N_k \times 3N_k$ matrices collecting, respectively, q_p, m_{ep}, m_{Ip}, k_{ep}, $\mathbb{K}_{pq}$, and b_{ep}. The equations of motion determine the amplitude response of the nuclear positions x_I and electronic dipole moments $p_e = Q_e x_e$ in the presence of an electric field, represented by a $3N_k$-dimensional vector e_e obtained by evaluating $|\mathbf{E}\rangle$ at every atomic position. Solving for $p_e = \alpha e_e$ yields the electric susceptibility matrix,

$$\alpha = Q_e[K_e - i\omega B_e - \omega^2 M_e$$
$$- K_e(K_e + K_I - \omega^2 M_I)^{-1}K_e]^{-1}Q_e, \qquad (5)$$

which enters the expansion of $\mathbb{V}_k$ above. The discrepancies in the masses of electronic and nuclear oscillators ensures that the poles of α separate into ultraviolet resonances, corresponding to predominantly electronic modes, and infrared resonances, corresponding to phononic modes, the latter of which is primarily responsible for thermal emission.

The form of K_I, coupling neighboring nuclei, ensures that nonlocality enters the polarization response in a microscopic rather than phenomenological manner. Hence, in contrast to point dipoles or macroscopic objects modeled via local susceptibilities [13,14,21,60,61], which lead to diverging EM fields as two or more bodies approach one another, the molecular susceptibility above will always be finite. In particular, the electronic response is accurately described by localized Gaussian basis functions [32,34,62–66],

$$f_p(\mathbf{x}) = (\sqrt{2\pi}\sigma_p)^{-3} \exp\left(-\frac{(\mathbf{x} - \mathbf{x}_p)^2}{2\sigma_p^2}\right), \qquad (6)$$

centered at the locations $\mathbf{x}_p$ of each atom p, normalized such that $\int d^3\mathbf{x} f_p = 1$, and featuring a width that, rather than being phenomenological [67,68], depends on the bare atomic polarizability at every frequency via $\sigma_p(\omega) = [(|\alpha_p(\omega)|/\sqrt{72\pi^3})]^{1/3}$ [32,69], where $\alpha_p(\omega) = \sum_{q,j}\alpha_{pj,qj}(\omega)$. [Note that the effective polarizability of each atom is defined as a trace over the delocalized susceptibility matrix arising from the solution of the above equations of motion (5); physically, it includes both short-range Coulombic electronic interactions and polarization smearing due to short-range ion-ion interactions (described by the spring matrix K_I).] Such basis functions mitigate short-distance EM divergences through the smearing of the response over nonzero widths σ_p, leading to finite matrix elements, $\langle f_p|(\cdots)f_q\rangle = \int d^3\mathbf{x} d^3\mathbf{x}' f_p(\mathbf{x})(\cdots)f_q(\mathbf{x}') < \infty$, even for coincident atoms $p = q$. While these widths are typically smaller than 1 Å [32,34] when phonons are ignored, we find that the introduction of phonons delocalizes the effective atomic polarization response in a way that depends strongly on the shapes of the molecules, leading to dramatically larger widths, on a scale $\xi \sim 1$ nm. As we show below, this stronger nonlocality has a noticeable impact on heat transfer among molecules at nanometric separations. Furthermore, since α enters $\mathbb{T}$, which includes long-range EM scattering, thermal fluctuations will be largest near the frequency poles of $\mathbb{T}$, corresponding to the dressed, phonon-polariton resonances of the fully coupled hybrid molecular-macroscopic system. Note that the root-mean-square amplitude of quantum-thermal fluctuations in x_e and x_I themselves is over 2 orders of magnitude smaller than the covalent bond length scale of an angstrom, so the equilibrium atomic positions $\mathbf{x}_p$ are essentially fixed.

Predictions.—We now exploit this framework to present new proof-of-concept predictions of thermal emission and heat transfer. For simplicity, we consider $\mathbb{G}_{env}$ as arising from the field response in either vacuum or above a gold plate, modeled as a perfect electrically conducting surface [70]. We consider either a C_{500} fullerene of radius 1 nm or a 500-atom-long carbyne wire of length 65 nm in various configurations above the plane. Where appropriate, we explicitly compare results obtained by evaluating the retarded many-body (RMB) transfer rates (1), which capture the impact of multiple scattering, molecular geometry, and EM screening to all orders, to those obtained from a dipolar approximation (DA) that contracts the bare molecular responses $\mathbb{V}$ into a point particle, with the susceptibilities and screened responses replaced by contracted dipolar polarizabilities $(\boldsymbol{\alpha}^\infty)_{ij} = \sum_{p,q}\alpha_{pi,qj}$. For convenience, the integrated powers are normalized to the emitted power $P_B = \sigma_B T^4 A$ of a blackbody of the same temperature T and area A. Within this approximation, the thermal emission rate of a molecule can be approximated (to lowest order in the scattering) by [Note that it is also possible to compare the RMB results against a DA that includes higher-order scattering effects [53], e.g. multiple scattering that becomes relevant in resonant situations; we find that thermal emission matches the RMB description as the molecules are far enough away from the conducting surface to be well-approximated as screened point dipoles, but near-field heat transfer in such a DA still does not match the RMB description due to neglect of the confluence of finite size and smeared nonlocal response relevant at shorter separations.]

$$\Phi_\infty^{(0)} = -\frac{1}{2\pi}\text{Tr}[\text{Im}\boldsymbol{\alpha}^\infty\text{Im}\mathbb{G}_{env}]. \qquad (7)$$

For a molecule at some position $\mathbf{r}_0 = z\mathbf{e}_z$ above the plate, $\text{Im}\mathbb{G}_{env}$ can be obtained from image theory; it is a constant in the near field and in the far field ($z \gg \omega/c$) given by $\text{Im}\mathbb{G}_{env}(\omega, z, z) = (\omega^3/6\pi c^3)\mathbb{I} - (\omega^2/8\pi c^2 z)\sin[(2\omega z/c)]\times(\mathbb{I} - \mathbf{e}_z \otimes \mathbf{e}_z)$.

Figure 1 shows the far-field thermal emission of either molecule at $T = 300$ K as a function of their distance z above the gold plate at zero kelvin, normalized by the emission rate P_B (on the order of 10^{-14} W) of blackbodies of the same effective areas. The C_{500} fullerene is a compact molecule whose vibrational modes and resulting polaritons are limited in extent by its small size. As a result, its emission spectrum consists of a small set of resonances in a narrow frequency range and is dominated by a single peak at $\omega_0 \approx 7 \times 10^{13}$ rad/s, causing the emission to scale as $z^{-1}\sin(2\omega_0 z/c)$ in the limit of $z \gg \lambda_T = (\hbar c/k_B T) \approx 7.6$ μm, where λ_T is the thermal wavelength. At small z, the emission approaches a constant value that is attenuated relative to vacuum by screening of the field response near the gold surface. Similar behavior is observed in the case of a carbyne wire parallel to the
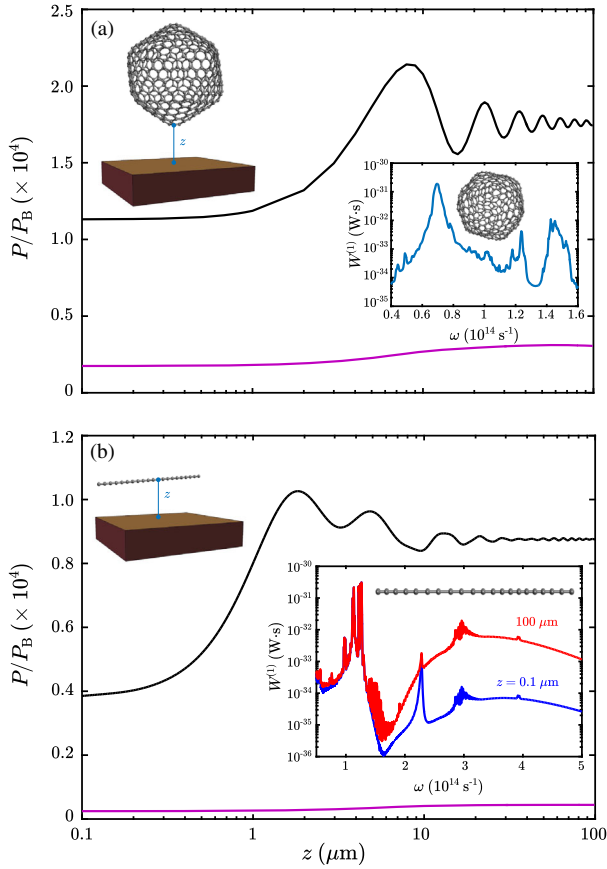
FIG. 1. Contribution of phonon polaritons to molecular thermal emission. (a) RMB (black) and DA (magenta) emission rates of a C_{500} fullerene held at $T = 300$ K above a zero-temperature gold plate as a function of vertical separation z, normalized by the power emitted by a blackbody of the same area $P_B = \sigma_B T^4 A$, where $A = 4\pi R^2$ and $R = 1$ nm. (Insets) A schematic of the fullerene above the plate as well as the RMB emission spectrum in the limit $z \to \infty$, along with a schematic of the dominant polaritonic mode. (b) Same as (a) but for a carbyne wire parallel to the plate, where $A = 2\pi RL$, $R = 0.13$ nm, and $L = 65$ nm. The RMB emission spectrum is shown at both $z = 0.1$ μm (blue) and $z = 100$ μm (red).
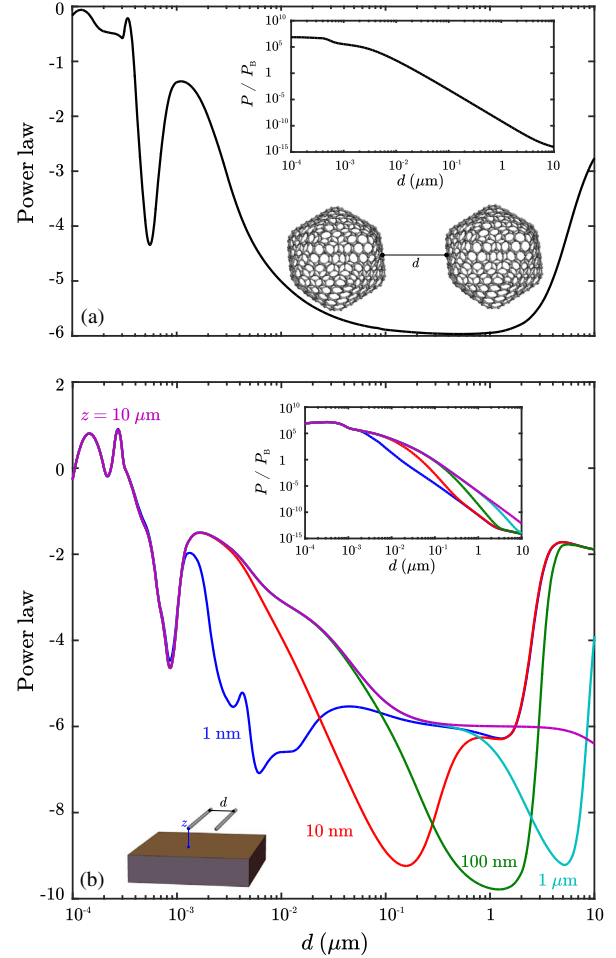

FIG. 2. Impact of nonlocal response, shape, and many-body effects on heat exchange between molecules. (a) Power law of heat transfer, $\partial(\log P)/\partial(\log d)$, between two C_{500} fullerenes in vacuum held at $T = 300$ and 0 K, with respect to their surface-surface separation d. (Inset) The transfer versus d, normalized by the emission rate from a corresponding room-temperature black-body P_B. (b) Same as (a) but for two 500-atom-long parallel carbyne wires oriented parallel to a gold plate. The various curves denote different values of their vertical distance z from the plate.

surface, except that the elongated shape of the molecule enables longer-range vibrational modes and stronger polarization anisotropy, which further suppresses emission at small z. For both molecules, the DA (7) underestimates the far-field emission by almost an order of magnitude for all z, due to the neglect of long-range EM scattering and screening effects. More dramatically, for the carbyne wire in the RMB treatment, as z increases, a set of closely spaced infrared polaritonic resonances begin to contribute, causing a beating pattern in the emission as a function of z. These close resonances do not arise within the DA, which only captures the impact of short-range EM interactions on the polarization response.

Figure 2 considers the heat transfer between two molecules, one at $T = 300$ K and the other at zero temperature,

as a function of their mutual horizontal separation d for several different values of their (identical) distances z above the zero-temperature plate. For two fullerenes far from the plate, we find that the flux rate transitions from $1/d^2$ in the far field to $1/d^6$ in the near field ($d \ll \lambda_T$), leading to flux rates $P \gg P_B$, consistent with the dipolar approximation [60,61]. However, as d decreases further to become comparable to the phonon-induced nonlocal length scale $\xi \sim 1$ nm, the EM response begins to probe the finite sizes and smeared electronic response of the molecules, causing the heat transfer to saturate (in contrast to the diverging flux rate arising in the dipolar picture) and the resulting power-law exponent to approach zero. Hence, (3) seamlessly captures the transition between radiation and conduction.

In the case of two parallel carbyne wires above a gold plate, the departures from dipolar and pairwise predictions are even more stark. For most separations d, as z decreases, the proximate surface severely attenuates the heat flux relative to vacuum (by over 4 orders of magnitude at $z \sim \xi$), except at very small values of $d \lesssim \xi \ll z$, where the overlapping nonlocal molecular response functions leads to saturation of the heat transfer independent of z. In the far field $d \gg \lambda_T$, as the molecules are much smaller than λ_T, the metal plate does not affect the heat transfer much, so the power law attains the far-field dipolar limit of -2, and the heat transfer powers converge for different z. As d decreases further, if $z \gg \lambda_T$, the power law reaches the near-field dipolar limit of -6, but if $z < \lambda_T$, the image dipoles induced in the proximate surface lead to an effective triple-dipole configuration with a power law of -9, akin to the so-called Axilrod-Teller-Muto correction for dipolar vdW interactions [30,32,71]. These power laws exhibit progressively stronger deviations from either the dipolar limit of -6 or the pairwise limit of -5 (obtained by summing the dipolar heat transfer between pairs of atoms across these parallel linear molecules) in the near field as d decreases further, due to the confluence of various competing length scales, including z, d, the wire lengths, ξ, and λ_T. If $z > \xi$, the heat transfer begins to saturate for $d \lesssim 10$ nm due to the nonlocal response, and the power laws are dominated by pairwise interactions of proximate dressed carbon atoms, so the power laws at each z match those of fullerenes in vacuum, as they are both carbon allotropes. The situation becomes more complicated when both, d, $z \lesssim \xi$ [72], due to the interplay of elongated molecular shapes, finite sizes, and nonlocal response of the wires and their images in the conducting surface. Note that, for $z < \xi$, the atomism of the conducting surface becomes more relevant and should also be treated, but this requires extending our current framework to handle periodically extended objects.

Concluding remarks.—We have demonstrated a mesoscopic approach to computing nonequilibrium thermal emission and radiative heat transfer among molecules in the presence of planar metallic surfaces, accounting for molecular nonlocal response as well as many-body and multiple scattering effects to all orders. Our approach demonstrates significant deviations in the emitted and transferred power from commonly used local or dipolar approximations, particularly in the near field and even at relatively large separations of 10 nm, where the modification to long-range EM interactions due to the proximate surface as well as the nonlocal molecular susceptibility both matter; moreover, it has the virtue of deriving atomic characteristics from *ab initio* DFT methods, in contrast to phenomenological treatments of nonlocal response [73–75], which give heat transfer results that depend strongly on the nonlocal material model and boundary conditions considered. Our approach can be generalized to consider extended materials like graphene or organic crystals, which might enable accurate computations of radiative contributions to bulk thermal conductivity beyond the Fourier regime, as well as actively studied experimental situations, including molecular materials in the vicinity of heated atomic force microscopy tips with applications to molecular junctions [7,8].

[1] R. Messina and P. Ben-Abdallah, Sci. Rep. **3**, 1383 (2013).

[2] V. B. Svetovoy and G. Palasantzas, Phys. Rev. Applied **2**, 034006 (2014).

[3] O. Ilic, M. Jablan, J. D. Joannopoulos, I. Celanovic, and M. Soljačić, Opt. Express **20**, A366 (2012).

[4] A. Lenert, D. M. Bierman, Y. Nam, W. R. Chan, I. Celanović, M. Soljačić, and E. N. Wang, Nat. Nanotechnol. **9**, 126 (2014).

[5] X. L. Ruan and M. Kaviany, Phys. Rev. B **73**, 155422 (2006).

[6] S. V. Boriskina, J. K. Tong, W.-C. Hsu, B. Liao, Y. Huang, V. Chiloyan, and G. Chen, Nanophotonics **5**, 134 (2016).

[7] L. Cui, R. Miao, C. Jiang, E. Meyhofer, and P. Reddy, J. Chem. Phys. **146**, 092201 (2017).

[8] L. Cui, W. Jeong, S. Hur, M. Matt, J. C. Klöckner, F. Pauly, P. Nielaba, J. C. Cuevas, E. Meyhofer, and P. Reddy, Science **355**, 1192 (2017).

[9] L. Cui, Y. Feng, and X. Zhang, J. Phys. Chem. A **119**, 11226 (2015).

[10] J. B. Pendry, K. Sasihithlu, and R. V. Craster, Phys. Rev. B **94**, 075414 (2016).

[11] S. Edalatpour and M. Francoeur, Phys. Rev. B **94**, 045406 (2016).

[12] V. Chiloyan, J. Garg, K. Esfarjani, and G. Chen, Nat. Commun. **6**, 6755 (2015).

[13] K. Kloppstech, N. Könne, S.-A. Biehs, A. W. Rodriguez, L. Worbes, D. Hellmann, and A. Kittel, Nat. Commun. **8**, 14475 (2017).

[14] L. Cui, W. Jeong, V. Fernández-Hurtado, J. Feist, F. J. García-Vidal, J. C. Cuevas, E. Meyhofer, and P. Reddy, Nat. Commun. **8**, 14479 (2017).

[15] R. St-Gelais, B. Guha, L. Zhu, S. Fan, and M. Lipson, Nano Lett. **14**, 6971 (2014).

[16] Z. Tian, K. Esfarjani, and G. Chen, Phys. Rev. B **89**, 235307 (2014).

[17] Z. Tian, K. Esfarjani, and G. Chen, Phys. Rev. B **86**, 235304 (2012).

[18] A. W. Rodriguez, M. T. H. Reid, and S. G. Johnson, Phys. Rev. B **88**, 054305 (2013).

[19] A. G. Polimeridis, M. T. H. Reid, W. Jin, S. G. Johnson, J. K. White, and A. W. Rodriguez, Phys. Rev. B **92**, 134202 (2015).

[20] H. Hajian, A. Ghobadi, S. A. Dereshgi, B. Butun, and E. Ozbay, J. Opt. Soc. Am. B **34**, D29 (2017).

[21] S. Shen, A. Narayanaswamy, and G. Chen, Nano Lett. **9**, 2909 (2009).

[22] F. J. García de Abajo, ACS Nano **7**, 11409 (2013).

[23] D. N. Basov, M. M. Fogler, and F. J. García de Abajo, Science **354**, aag1992 (2016).

[24] T. Luo and G. Chen, Phys. Chem. Chem. Phys. **15**, 3389 (2013).

[25] V. P. Carey, G. Chen, C. Grigoropoulos, M. Kaviany, and A. Majumdar, Nanoscale Micro. Thermophys. Eng. **12**, 1 (2008).

[26] S. V. Boriskina, H. Ghasemi, and G. Chen, Mater. Today **16**, 375 (2013).

[27] D. G. Cahill, P. V. Braun, G. Chen, D. R. Clarke, S. Fan, K. E. Goodson, P. Keblinski, W. P. King, G. D. Mahan, A. Majumdar, H. J. Maris, S. R. Phillpot, E. Pop, and L. Shi, Appl. Phys. Rev. **1**, 011305 (2014).

[28] A. Dhar and D. Roy, J. Stat. Phys. **125**, 801 (2006).

[29] N. Mingo and L. Yang, Phys. Rev. B **68**, 245406 (2003).

[30] A. Tkatchenko, A. Ambrosetti, and R. A. DiStasio, Jr., J. Chem. Phys. **138**, 074106 (2013).

[31] V. V. Gobre and A. Tkatchenko, Nat. Commun. **4**, 2341 (2013).

[32] R. A. DiStasio, Jr., V. V. Gobre, and A. Tkatchenko, J. Phys. Condens. Matter **26**, 213202 (2014).

[33] A. Tkatchenko, Adv. Funct. Mater. **25**, 2054 (2015).

[34] A. Ambrosetti, N. Ferri, R. A. DiStasio, Jr., and A. Tkatchenko, Science **351**, 1171 (2016).

[35] A. Henry and G. Chen, Phys. Rev. Lett. **101**, 235502 (2008).

[36] K. Esfarjani, G. Chen, and H. T. Stokes, Phys. Rev. B **84**, 085204 (2011).

[37] E. G. Noya, D. Srivastava, L. A. Chernozatonskii, and M. Menon, Phys. Rev. B **70**, 115416 (2004).

[38] R. Messina, M. Tschikin, S.-A. Biehs, and P. Ben-Abdallah, Phys. Rev. B **88**, 104307 (2013).

[39] A. Pérez-Madrid, J. M. Rubí, and L. C. Lapas, Phys. Rev. B **77**, 155417 (2008).

[40] S. Edalatpour and M. Francoeur, J. Quant. Spectrosc. Radiat. Transfer **133**, 364 (2014).

[41] S. Edalatpour, J. DeSutter, and M. Francoeur, J. Quant. Spectrosc. Radiat. Transfer **178**, 14 (2016).

[42] R. Yu, A. Manjavacas, and F. J. G. de Abajo, Nat. Commun. **8**, 2 (2017).

[43] M. Krüger, G. Bimonte, T. Emig, and M. Kardar, Phys. Rev. B **86**, 115423 (2012).

[44] S. Molesky and Z. Jacob, Phys. Rev. B **91**, 205435 (2015).

[45] B. Zhao, B. Guizal, Z. M. Zhang, S. Fan, and M. Antezza, Phys. Rev. B **95**, 245437 (2017).

[46] C. R. Otey, L. Zhu, S. Sandhu, and S. Fan, J. Quant. Spectrosc. Radiat. Transfer **132**, 3 (2014).

[47] M. T. H. Reid, A. W. Rodriguez, and S. G. Johnson, Proc. IEEE **101**, 531 (2013).

[48] A. W. Rodriguez, O. Ilic, P. Bermel, I. Celanovic, J. D. Joannopoulos, M. Soljačić, and S. G. Johnson, Phys. Rev. Lett. **107**, 114302 (2011).

[49] C. Luo, A. Narayanaswamy, G. Chen, and J. D. Joannopoulos, Phys. Rev. Lett. **93**, 213905 (2004).

[50] M. Jablan, M. Soljačić, and H. Buljan, Phys. Rev. B **83**, 161409 (2011).

[51] E. H. Hwang, R. Sensarma, and S. Das Sarma, Phys. Rev. B **82**, 195406 (2010).

[52] S. Xiao, X. Zhu, B.-H. Li, and N. A. Mortensen, Frontiers Phys. **11**, 117801 (2016).

[53] P. S. Venkataram, J. Hermann, A. Tkatchenko, and A. W. Rodriguez, Phys. Rev. Lett. **118**, 266802 (2017).

[54] B. Song, Y. Ganjeh, S. Sadat, D. Thompson, A. Fiorino, V. Fernández-Hurtado, J. Feist, F. J. Garcia-Vidal, J. C. Cuevas, P. Reddy et al., Nat. Nanotechnol. **10**, 253 (2015).

[55] See Supplemental Material at http://link.aps.org/supplemental/10.1103/PhysRevLett.121.045901, which also cites Ref. [56], for a derivation of (1) along with further details on the molecular susceptibility parameters.

[56] L. Novotny and B. Hecht, Principles of Nano-Optics (Cambridge University Press, Cambridge, England, 2006), p. 335.

[57] S. J. Rahi, T. Emig, N. Graham, R. L. Jaffe, and M. Kardar, Phys. Rev. D **80**, 085021 (2009).

[58] A. Ambrosetti, A. M. Reilly, R. A. DiStasio, and A. Tkatchenko, J. Chem. Phys. **140**, 18A508 (2014).

[59] S. Y. Buhmann, S. Scheel, S. A. Ellingsen, K. Hornberger, and A. Jacob, Phys. Rev. A **85**, 042513 (2012).

[60] A. I. Volokitin and B. N. J. Persson, Phys. Rev. B **63**, 205404 (2001).

[61] G. Domingues, S. Volz, K. Joulain, and J.-J. Greffet, Phys. Rev. Lett. **94**, 085901 (2005).

[62] A. G. Donchev, J. Chem. Phys. **125**, 074713 (2006).

[63] A. D. Phan, L. M. Woods, and T.-L. Phan, J. Appl. Phys. **114**, 044308 (2013).

[64] Y. V. Shtogun and L. M. Woods, J. Phys. Chem. Lett. **1**, 1356 (2010).

[65] H.-Y. Kim, J. O. Sofo, D. Velegol, M. W. Cole, and A. A. Lucas, Langmuir **23**, 1735 (2007).

[66] M. W. Cole, D. Velegol, H.-Y. Kim, and A. A. Lucas, Mol. Simul. **35**, 849 (2009).

[67] J. Mahanty and B. W. Ninham, J. Chem. Soc., Faraday Trans. 2 **71**, 119 (1975).

[68] M. J. Renne, Physica (Utrecht) **53**, 193 (1971).

[69] A. Mayer, Phys. Rev. B **75**, 045407 (2007).

[70] For computational convenience, and since gold is essentially perfectly reflecting at infrared frequencies where nonequilibrium energy transfer is most significant, we model the gold plate as a perfect electrically conducting surface.

[71] B. M. Axilrod and E. Teller, J. Chem. Phys. **11**, 299 (1943).

[72] Note that, in principle, as d attains angstrom length scales, the assumption of the molecules being separate breaks down due to the possible formation of new covalent bonds; while this would require recomputing K_I for the coupled molecular system, our formalism for computing radiative heat transfer still holds as long as the two molecular components can be maintained at different temperatures.

[73] P.-O. Chapuis, S. Volz, C. Henkel, K. Joulain, and J.-J. Greffet, Phys. Rev. B **77**, 035431 (2008).

[74] F. Singer, Y. Ezzahri, and K. Joulain, J. Quant. Spectrosc. Radiat. Transfer **154**, 55 (2015).

[75] R. Schmidt and S. Scheel, J. Phys. B **51**, 044003 (2018).